

Generalized Equalization Model for Image Enhancement

Hongteng Xu, Guangtao Zhai, *Member, IEEE*, Xiaolin Wu, *Fellow, IEEE*, and Xiaokang Yang, *Senior Member, IEEE*

Abstract—In this paper, we propose a generalized equalization model for image enhancement. Based on our analysis on the relationships between image histogram and contrast enhancement/white balancing, we first establish a generalized equalization model integrating contrast enhancement and white balancing into a unified framework of convex programming of image histogram. We show that many image enhancement tasks can be accomplished by the proposed model using different configurations of parameters. With two defining properties of histogram transform, namely contrast gain and nonlinearity, the model parameters for different enhancement applications can be optimized. We then derive an optimal image enhancement algorithm that theoretically achieves the best joint contrast enhancement and white balancing result with trading-off between contrast enhancement and tonal distortion. Subjective and objective experimental results show favorable performances of the proposed algorithm in applications of image enhancement, white balancing and tone correction. Computational complexity of the proposed method is also analyzed.

Index Terms—Contrast enhancement, contrast gain, generalized equalization, nonlinearity of transform, tone mapping, white balancing.

I. INTRODUCTION

WITH the fast advance of technologies and the prevalence of imaging devices, billions of digital images are being created every day. Due to undesirable light source, unfavorable weather or failure of the imaging device itself, the contrast and tone of the captured image may not always be satisfactory. Therefore, image enhancement is often required for both the aesthetic and pragmatic purposes. In fact, image enhancement algorithms have already been widely applied in imaging devices for tone mapping. For example, in a typical digital camera, the CCD or CMOS array receives the photons passing through lens and then the charge levels are transformed to the original image.

Manuscript received December 12, 2012; revised May 18, 2013; accepted July 04, 2013. Date of publication September 25, 2013; date of current version December 12, 2013. This work was supported in part by NSFC (60932006, 61025005, 61001145, 61129001, 61221001, 61371146) and the 111 Project (B07022). The associate editor coordinating the review of this manuscript and approving it for publication was Dr. Xiao-Ping Zhang.

H. Xu, G. Zhai, and X. Yang are with the Institute of Image Communication and Information Processing, Shanghai Jiao Tong University, Shanghai 200240, China (e-mail: hongtengxu@sjtu.edu.cn; zhaiguangtao@sjtu.edu.cn; xkyang@sjtu.edu.cn).

X. Wu is with the Department of Electrical & Computer Engineering, McMaster University, Hamilton, ON L8G 4K1, Canada, and also with the Institute of Image Communication and Information Processing, Shanghai Jiao Tong University, Shanghai 200240, China (e-mail: xwu@ece.mcmaster.ca).

Color versions of one or more of the figures in this paper are available online at <http://ieeexplore.ieee.org>.

Digital Object Identifier 10.1109/TMM.2013.2283453

Usually, the original image is stored in RAW format, with a bit-length too big for normal displays. So tone mapping techniques, e.g. the widely known gamma correction, are used to transfer the image into a suitable dynamic range. More sophisticated tone mapping algorithms were developed through the years, see [2], [8], [12], [29], [33], [34], [43], just to name a few.

Generally, tone mapping algorithms can be classified into two categories by their functionalities during the imaging process.

1) *White Balancing*: Because of the undesirable illuminance or the physical limitations of inexpensive imaging sensors, the captured image may carry obvious color bias.¹ To calibrate the color bias of image, we need to estimate the value of light source, the problem of which called color constancy [16], [18], [21], [40], [41]. Using a suitable physical imaging model, one can get an approximated illuminance, and then a linear transform can be applied to map the original image into an ideal one.

2) *Contrast Enhancement*: Contrast enhancement algorithms are widely used for the restoration of degraded media, among which global histogram equalization is the most popular choice. Other variants includes local histogram equalization [42] and the spatial filtering type of methods [11], [14], [27], [32], [39], [44]. For example, in [32] the fractional filter is used to promote the variance of texture so as to enhance the image. In [31], a texture synthesis based algorithm is proposed for degraded media, such as old pictures or films. On the other hand, transform based methods also exist, e.g. curvelet based algorithm in [35]. In [44], an adaptive steering regression kernel is proposed to combine image sharpening with denoising.

Despite of the abundant literature on image enhancement, including those representatives listed above, two challenging problems for image enhancement are still not solved. First, *how to achieve contrast enhancement while preserving a good tone*. The contrast and tone of an image have mutual influence. Because of the complicated interaction, those algorithms merely aiming towards contrast enhancement or white balancing cannot provide optimal visual effect. Most, if not all, of current image enhancement systems divide white balancing and contrast enhancement into two separate and independent phases, as Fig. 1(a) shows. This strategy has an obvious drawback: although tone has adjusted in the white balancing phase, contrast enhancement may undesirably bias it again. This trouble has been observed in many applications, e.g. the de-hazing algorithms in [26], [37], [38] achieve contrast enhancement by

¹In fact, the color bias is caused by tone distortions of the three channels, so “tone” in this paper is referring not only to gray image, but also the hue of color image. We will not explicitly discriminate these two concepts in this work.

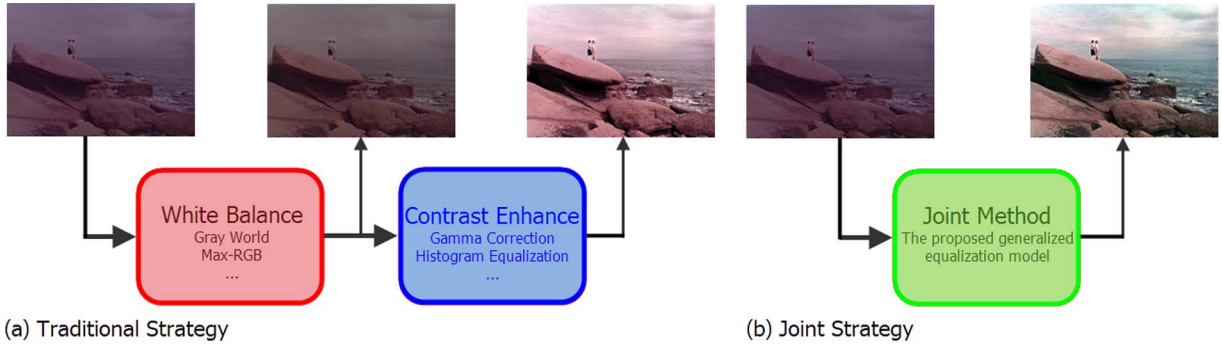


Fig. 1. Figure (a) is the illustration of traditional image enhancement strategy. Figure (b) is the illustration of joint image enhancement strategy.

increasing saturation of the image, but cause tonal distortion in some cases. It is easy to imagine that joint white balancing and contrast enhancement, as Fig. 1(b) shows, is a more efficient solution towards overall quality enhancement.

Second, *how to theoretically relate different types of enhancement algorithms to each other*. In this aspect, the work in [30] unifies spatial filtering based enhancement methods, including bi-lateral filter, non-local means filter, steering regression and so on, which has potential applications in image enhancement. However, the computational complexity of filtering based method is much higher than traditional histogram based method in most situations. In many cases, such as real-time video surveillance, the histogram based methods are still being widely used. Taking its significance in practical situations into consideration, finding a unified framework of histogram based methods is a meaningful work that may bring more inspirations to the image enhancement problem and facilitate future research. Although being originated from different applications, both of contrast enhancement and white balancing are essentially tone manipulation processes. In fact, it is noticed that almost all global algorithms of contrast enhancement and white balancing are based on histogram transform. Recently, a unified model for color constancy is proposed in [40] based on the concept of low-level visual information. However, this unified model does not take contrast into consideration, so it is limited to the application of white balancing. Wu [43] introduced a strict definition of expected context-free contrast and devised a method called Optimal Contrast-Tone Mapping (OCTM) to solve contrast enhancement problem by maximizing the expected contrast gain subject to an upper limit on tone distortion. OCTM is a promising solution for the intensity channel, but it does not elucidate the relationship between contrast and tone on the color channels.

In this paper, we will analyze the relationships between image histogram and tone/contrast of image, and establish a generalized equalization model. We will propose a series of definitions for context-free contrast, tone distortion and its nonlinearity, and clarify their relationships in terms of different parameters in the unified model. The generalized equalization model amalgamates histogram-based tone mapping algorithms in a generalized framework of convex programming and therefore is a joint strategy as shown in Fig. 1(b). Extensive experimental results show that the proposed method can be widely used in a series of enhancement applications with promising results.

The rest of the paper is organized as follows. In Section II, we establish the relationship between histogram and contrast/tone of images. It is shown that white balancing is realized by the linear transform of histogram, while contrast enhancement is achieved by the nonlinear transform of histogram, and both of which are generalized in the proposed model. In Section III, we give rigorous analysis of the choice of parameters in the model. Experimental results are given in Section IV, and Section V concludes the paper.

II. GENERALIZED EQUALIZATION MODEL

Consider an image $\mathbf{f} = (f_r, f_g, f_b)^T$. The available dynamic range of f_c is $[0, L_c]$, $c = r, g, b$. The histogram of image is denoted as $\{\mathbf{h}_c, \mathbf{p}_c\}_{c=r,g,b}$. Here, $\mathbf{h}_c \in R^K$ represents the total K intensity levels, which corresponds to probability vector $\mathbf{p}_c \in R^K$. K is the number of intensity level whose probability value is non-zero. Given the histogram of original image, denoted as $\{\tilde{\mathbf{h}}_c, \mathbf{p}_c\}_{c=r,g,b}$, we achieve image enhancement by manipulating the histogram to be $\{\hat{\mathbf{h}}_c, \mathbf{p}_c\}_{c=r,g,b}$. The distance between adjacent intensity levels is denoted as $s_{ck} = h_{ck} - h_{c,k-1}$, $k = 2, \dots, K$, $s_{c1} = h_{c1}$. According to this denotation, we have $\tilde{\mathbf{s}}_c = \nabla \tilde{\mathbf{h}}_c$, $\hat{\mathbf{s}}_c = \nabla \hat{\mathbf{h}}_c$. ∇ represents derivation operator.

A. Histogram-Based Analysis on White Balancing

White balancing is a popular image enhancement method, with a critical step of color constancy. Being different from the learning based methods in [15], [16], [18], [21], [41], we focus on a low-level approach to color constancy and establish the relationship between color constancy and the histogram of image.

In the Lambertian surface model, the image is expressed as

$$f_c = \int r(\lambda)l(\lambda)m_c(\lambda)d\lambda. \quad (1)$$

Here, λ is the wavelength of visible light. $r(\lambda)$ is the surface reflectance, $l(\lambda)$ is the light source, and $m_c(\lambda)$ is the sensitivity of camera in the channel c . The goal of color constancy is to estimate the projection of light source on the RGB space. To achieve this goal, many assumptions have been made. For example, the max-RGB is proposed in [28], which estimates the light source from the maximum responses of the three channels. Another widely used assumption is gray-world hypothesis [4], which assumes that the average reflectance in the scene is

achromatic. Recently, these assumptions are unified in [17], as follows

$$\left(\frac{\int |\mathbf{f}(\mathbf{x})|^\alpha d\mathbf{x}}{\int d\mathbf{x}} \right)^{\frac{1}{\alpha}} = C\mathbf{e}. \quad (2)$$

Here, \mathbf{x} is the coordinate of pixel. C is an arbitrary positive constant and α is a parameter. $\mathbf{e} = [e_r, e_g, e_b]^T$ is the normalized estimation of light source. When $\alpha = 1$ (2) is equivalent to Gray-world assumption while when $\alpha = \infty$ (2) is equivalent to max-RGB. White balancing is achieved by multiplying the element of \mathbf{e} to the corresponding channel of \mathbf{f} . Because $[1/\sqrt{3}, 1/\sqrt{3}, 1/\sqrt{3}]^T$ is the normalized form of white light, the multiplication factor of channel c is $1/e_c\sqrt{3}$.

From the viewpoint of image histogram, the left side of (2) can be rewritten as

$$\left(\frac{\int |\mathbf{f}(\mathbf{x})|^\alpha d\mathbf{x}}{\int d\mathbf{x}} \right)^{\frac{1}{\alpha}} = \begin{pmatrix} (\mathbf{p}_r^T \mathbf{h}_r^\alpha)^{\frac{1}{\alpha}} \\ (\mathbf{p}_g^T \mathbf{h}_g^\alpha)^{\frac{1}{\alpha}} \\ (\mathbf{p}_b^T \mathbf{h}_b^\alpha)^{\frac{1}{\alpha}} \end{pmatrix}, \quad (3)$$

where $\mathbf{h}_c^\alpha = [h_{c1}^\alpha, \dots, h_{cK}^\alpha]^T$. Eq. (3) reveals the interconnection among white balancing and histogram. Given an image, \mathbf{e} is calculated as

$$e_c(\alpha) = \frac{(\mathbf{p}_c^T \tilde{\mathbf{h}}_c^\alpha)^{\frac{1}{\alpha}}}{\sqrt{\sum_{c=r,g,b} (\mathbf{p}_c^T \tilde{\mathbf{h}}_c^\alpha)^{\frac{2}{\alpha}}}}. \quad (4)$$

As a result, the histogram of white balancing result, denoted as $\hat{\mathbf{h}}_c$, is computed as follows

$$\hat{\mathbf{h}}_c = \frac{1}{e_c(\alpha)\sqrt{3}} \tilde{\mathbf{h}}_c. \quad (5)$$

It is obvious that this process is linear. The linearity of the transform is the most significant feature of histogram-based white balancing algorithm. In the next subsection, we will show that this linearity is also an important difference between white balancing and contrast enhancement.

B. Histogram-Based Analysis on Contrast Enhancement

In [43], the expected context-free contrast of image is defined by

$$\mathbf{C} = \mathbf{p}_c^T \mathbf{s}_c. \quad (6)$$

By the definition, the maximum contrast is L_c , which is achieved by a binary black-and-white image; the minimum contrast is zero when the image is a constant. So, the contrast enhancement is achieved by maximizing (6) in [43], as follows.

$$\begin{aligned} \hat{\mathbf{s}}_c &= \arg \max_{\mathbf{s}_c} \mathbf{p}_c^T \mathbf{s}_c, \\ \text{s.t. } &\sum_{i=1}^K s_{ci} = L_c, \quad s_{ci} \geq d, \end{aligned} \quad (7)$$

where the first constraint makes sure that the output image still has a suitable dynamic range and the second constraint denotes the minimum distance between adjacent gray levels as d .

However, although the definition in (6) has obvious statistical meaning, it is not optimal to be used as objective function directly. Eq. (7) is a linear programming problem whose solution is sparse—to the maximum probability p_{ci} , the corresponding $\hat{s}_{ci} = L_c - d(K-1)$, and other $\hat{s}_{cj} = d$. Realizing this problem, another two constraints are added in [43] to suppress artifacts, which makes the model complicated and sensitive to some predefined parameters.

Before the work in [43], histogram-based algorithm has been widely used in contrast enhancement. The most commonly used approach is histogram equalization [22], which makes the probability density function of enhanced image close to that of uniform distribution. After equalization, the i th intensity level of new image, \hat{h}_{ci} , is

$$\hat{h}_{ci} = C \sum_{j=0}^i p_{cj}. \quad (8)$$

Here, C is a constant. Eq. (8) also gives a relationship between histogram and the distance between adjacent intensity level, as following shows.

$$\hat{s}_{ci} = \hat{h}_{ci} - \hat{h}_{c,i-1} = Cp_{ci}. \quad (9)$$

According to (8), (9), histogram equalization is equivalent to solving following optimization problem.

$$\begin{aligned} \hat{\mathbf{s}}_c &= \arg \max_{\mathbf{s}_c} \frac{1}{\|\mathbf{P}_c^{-1} \mathbf{s}_c\|_\infty}, \\ \text{s.t. } &\sum_{i=1}^K s_{ci} = L_c, \quad s_{ci} \geq d. \end{aligned} \quad (10)$$

Here $\mathbf{P}_c = \text{diag}(p_{c1}, \dots, p_{cK})$.

The performance of histogram equalization is not optimal in most situations. The essential reason for its limited performance is the questionable assumption that the histogram of ideal image obeys uniform distribution. To get better equalization result, we need to find a better distribution which is a big challenge. Recently, some adaptive histogram equalization methods are proposed in [1], [5], [7], [24], [36] but gave neither a clear definition of contrast nor an explicit objective function of contrast enhancement like (7), (10) shows. A common feature of all the enhancement methods mentioned above is that the transform of histogram is non-linear, which is different from white balancing.

C. The Proposed Model

The aims of establishing the generalized equalization model include: 1) giving a unified explanation to white balancing problem and contrast enhancement problem; 2) providing an explicit objective function for these two problems and proposing a joint algorithm for them; 3) controlling the performance of the algorithm by as few parameters as possible.

The proposed model is inspired by (7), (10). Although (7), (10) seem to be very different, if we regard the order of \mathbf{P}_c and

the norm of the objective function as two parameters, β and n , (7), (10) are rewritten in a generalized form:

$$\begin{aligned} \hat{\mathbf{s}}_c &= \arg \max_{\mathbf{s}_c} \frac{1}{\|\mathbf{P}_c^{-\beta} \mathbf{s}_c\|_n}, \\ \text{s.t. } \sum_{i=1}^K s_{ci} &= L_c, \quad s_{ci} \geq d. \end{aligned} \quad (11)$$

Both (10) and (7) have interesting relationships with (11). When $n = 2$ and $\beta = 0.5$ (or $n = \infty$ and $\beta = 1$), maximum is reached when $s_{ci}/(p_{ci})^\beta = C$, which is equivalent (10). When $n = 2$ and $0 \leq \beta < 0.5$ (or $n = \infty$ and $0 \leq \beta < 1$), the solution would be smoother than that of (10). When $n = 1$ or $\beta \rightarrow \infty$, the solution is equivalent to that of (7). Compared with traditional histogram equalization, (11) is more flexible, because the target histogram does not have to obey uniform distribution. Considering the fact that traditional histogram equalization often leads to over-enhanced results, relaxing the constraints of uniform distribution can suppress over-enhancement effectively. On the other hand, as long as $n > 1$ and β in the suitable range, histogram of the enhanced image can avoid to be too sparse. As a result, we do not need additional constraints like OCTM does.

According to the analysis above, (11) provides a reasonable and unified definition with the objective function of contrast enhancement. We will further take white balancing into the model. Based on (4), (11), we formulate the generalized equalization model mathematically as follows.

$$\begin{aligned} \hat{\mathbf{s}}_c &= \arg \min_{\mathbf{s}_c} \sum_{c=r,g,b} \|\mathbf{P}_c^{-\beta} \mathbf{s}_c\|_n, \\ \text{s.t. } \sum_{i=1}^K s_{ci} &= \frac{1}{e_c(\alpha)\sqrt{3}} \sum_{i=1}^K \tilde{s}_{ci}, \quad s_{ci} \geq d. \end{aligned} \quad (12)$$

Here, \tilde{s}_c is the original distance between adjacent intensity levels of the channel c . In generalized model, we set the upper bound L_c as the result of white balancing $1/e_c(\alpha)\sqrt{3} \sum_{i=1}^K \tilde{s}_{ci}$.

On the top of (12), we introduce two measures into generalized equalization model: the gain of expected context-free contrast and the nonlinearity of the transform from $\tilde{\mathbf{h}}_c$ to $\hat{\mathbf{h}}_c$, which are defined as

$$\mathbf{G} = \frac{\mathbf{P}_c^T \hat{\mathbf{s}}_c}{\mathbf{P}_c^T \tilde{\mathbf{s}}_c}, \quad \mathbf{NL} = \|\nabla(\hat{\mathbf{s}}_c - \tilde{\mathbf{s}}_c)\|_2. \quad (13)$$

If $\tilde{\mathbf{s}}_c$ is homogeneous enough, $\mathbf{NL} \approx \|\nabla \hat{\mathbf{s}}_c\|_2$. The larger \mathbf{NL} , the stronger nonlinearity of the transform. The nonlinearity of white balancing methods is close to 0. On the other hand, the contrast enhancement methods often have strong nonlinearity, which achieve visible enhancement of contrast. However, separate nonlinear transform of histograms of three channels may cause tone distortion. In the next section, we will theoretically prove that the proposed method, with a suitable configuration of parameters, can achieve a best trade-off between contrast enhancement and tone adjustment.

TABLE I
THE LIST OF IMPORTANT VARIABLES IN THE MODEL

Variables	Descriptions
$\tilde{\mathbf{h}} \in R^K$	The intensity levels of original image
$\hat{\mathbf{h}} \in R^K$	The intensity levels of enhanced image
$\tilde{\mathbf{s}} \in R^K$	The distance of adjacent intensity levels of original image
$\hat{\mathbf{s}} \in R^K$	The distance of adjacent intensity levels of enhanced image
$\mathbf{p} \in R^K$	The probability of intensity level
$\mathbf{P} \in R^{K \times K}$	The diagonal matrix of \mathbf{p}
L	The upper bound of intensity
d	The lower bound of distance
$\mathbf{e}(\alpha)$	The estimated light source for original image
α	The parameter of color constancy
β	The parameter of nonlinearity
n	The parameter of norm
\mathbf{G}	Contrast Gain
\mathbf{NL}	Nonlinearity of transform

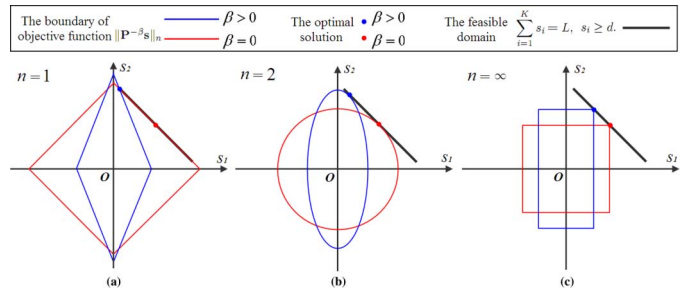


Fig. 2. In each sub-figure, the thick black line represents the feasible domain of Eq. (12); the red and blue wireframes show the boundaries of the objective function of Eq. (12) which correspond to the $\beta = 0$ and $\beta > 0$ situations respectively; the red and blue points are the optimal solutions corresponding to the $\beta = 0$ and $\beta > 0$ situations respectively. The parameter n in (a), (b), (c) is 1, 2 and ∞ respectively.

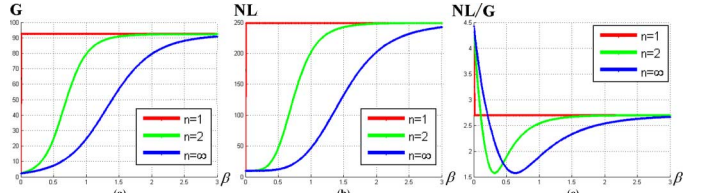


Fig. 3. Figure (a) gives the curves of contrast gain with the increase of β . Figure (b) gives the curves of nonlinearity of transform with the increase of β . Figure (c) gives the curves of the ratio of \mathbf{NL}_n to \mathbf{G}_n , $n = 1, 2, \infty$. The red, green and blue curves corresponding to $n = 1, 2, \infty$, respectively.

III. THE CONFIGURATION OF PARAMETERS

For the convenience of reading and analysis, we sum up the important variables and parameters with short descriptions of their roles in Table I.

A. The Choice of n and β

The choice of n has great influences on that of β and vice versa, so we will discuss them together. We first give a toy model in the 2D situation, as Fig. 2 shows. In the 2D situation, $\mathbf{s} = [s_1, s_2]$, $\mathbf{p} = [p_1, p_2]$ and we can assume $p_1 < p_2$ without loss of generality.

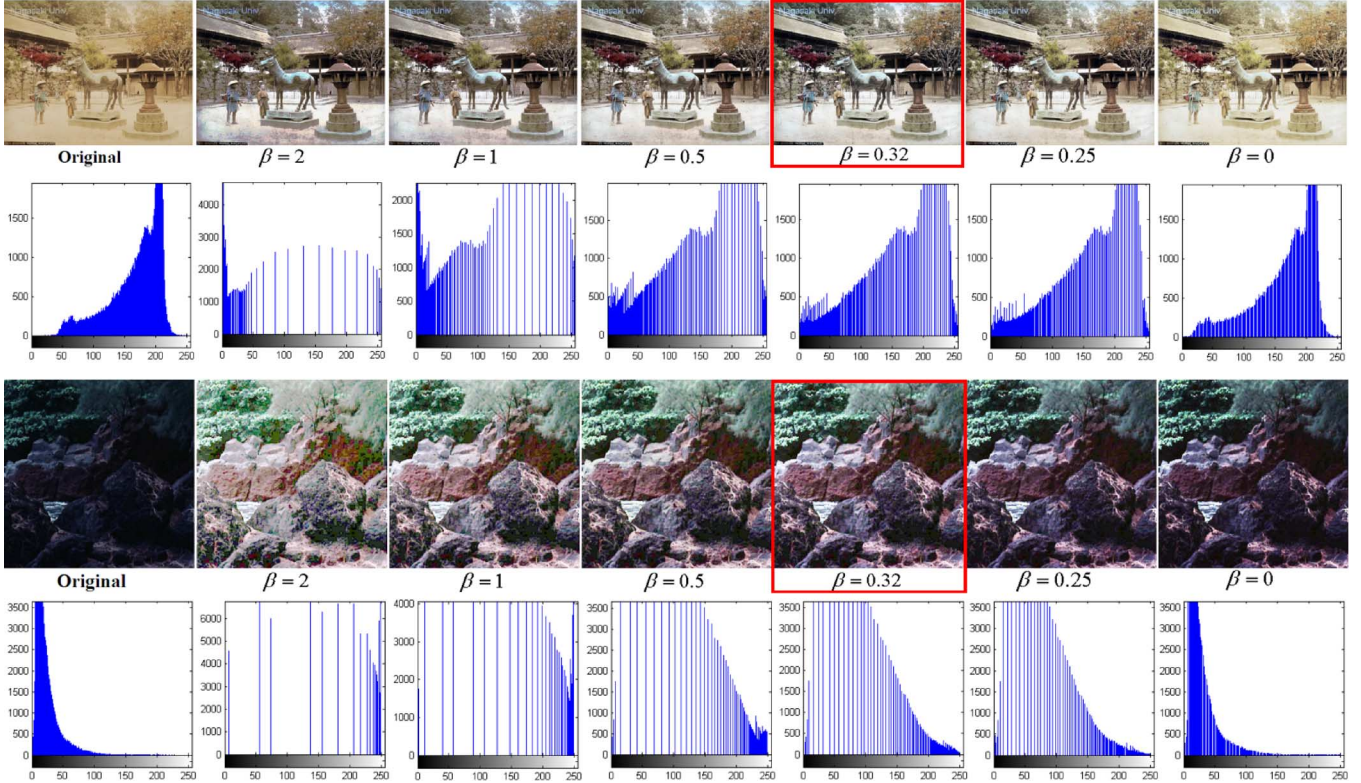


Fig. 4. The Figures give the enhancement results and the corresponding histograms with different β values.

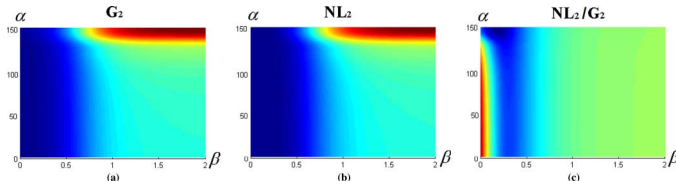


Fig. 5. Figure (a), (b) and (c) give the contrast gain, the nonlinearity of transform and the ratio between them in the $\alpha\beta$ -plane respectively. The α -axis is from 1 to 150 and the β -axis is from 0 to 2. The blue region represents low values while the red region represents high values.

TABLE II
THE DIFFERENT CONFIGURATIONS OF PARAMETERS

Function Tendency	$ n $	$ \alpha $	$ \beta $	Equivalent
Contrast Enhancement	$ \infty $	-	1	Histogram equalization [22]
Contrast Enhancement	2	-	0.5	Histogram equalization [22]
Contrast Enhancement	1	-	1	OCTM [43]
White Balance	$ \infty $	$ \infty $	0	maxRGB [28]
White Balance	$ \infty $	1	0	Gray world [4]
White Balance	$ \infty $	7	0	Shades of Gray (using α -th norm)[17]

In (12), n determines which Minkowski norm is used while β controls the shape of the ball in l_n space. Fig. 2 gives the boundaries of balls of $\|\mathbf{P}^{-\beta}\mathbf{s}\|_n$ with different β values. When $\beta = 0$, we have $\mathbf{P}^{-\beta}\mathbf{s} = \mathbf{s}$, the ball in the l_n space ($n = 1, 2, \infty$) is centrosymmetric. In such a situation, the optimal solution of (12) is reached as $s_i = L/2$. We can extend the conclusion to the general situation and then get following theorem.²

²Detailed proof of Theorem 1 and Theorem 2 are given in the Appendix.

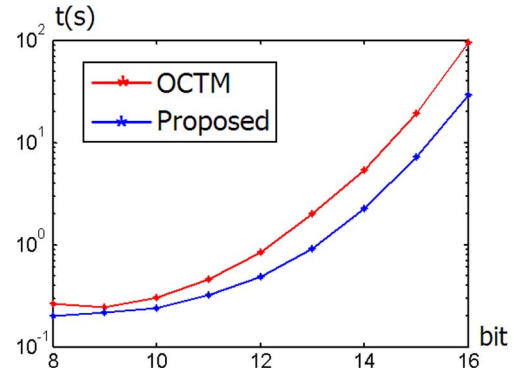


Fig. 6. The red curve corresponds to the processing time of OCTM [43] while the blue one corresponds to the processing time of the proposed method.

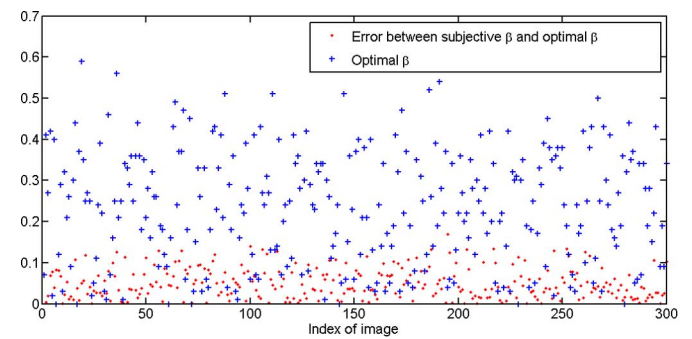


Fig. 7. The blue crosses show the $\hat{\beta}$ s for 300 images, and the red points show the average errors between subjective β and $\hat{\beta}$.

Theorem 1: In the case of $\beta = 0$, the minima of $\|\mathbf{P}^{-\beta}\mathbf{s}\|_n$ is reached when $s_i = L/K$, $i = 1, \dots, K$.

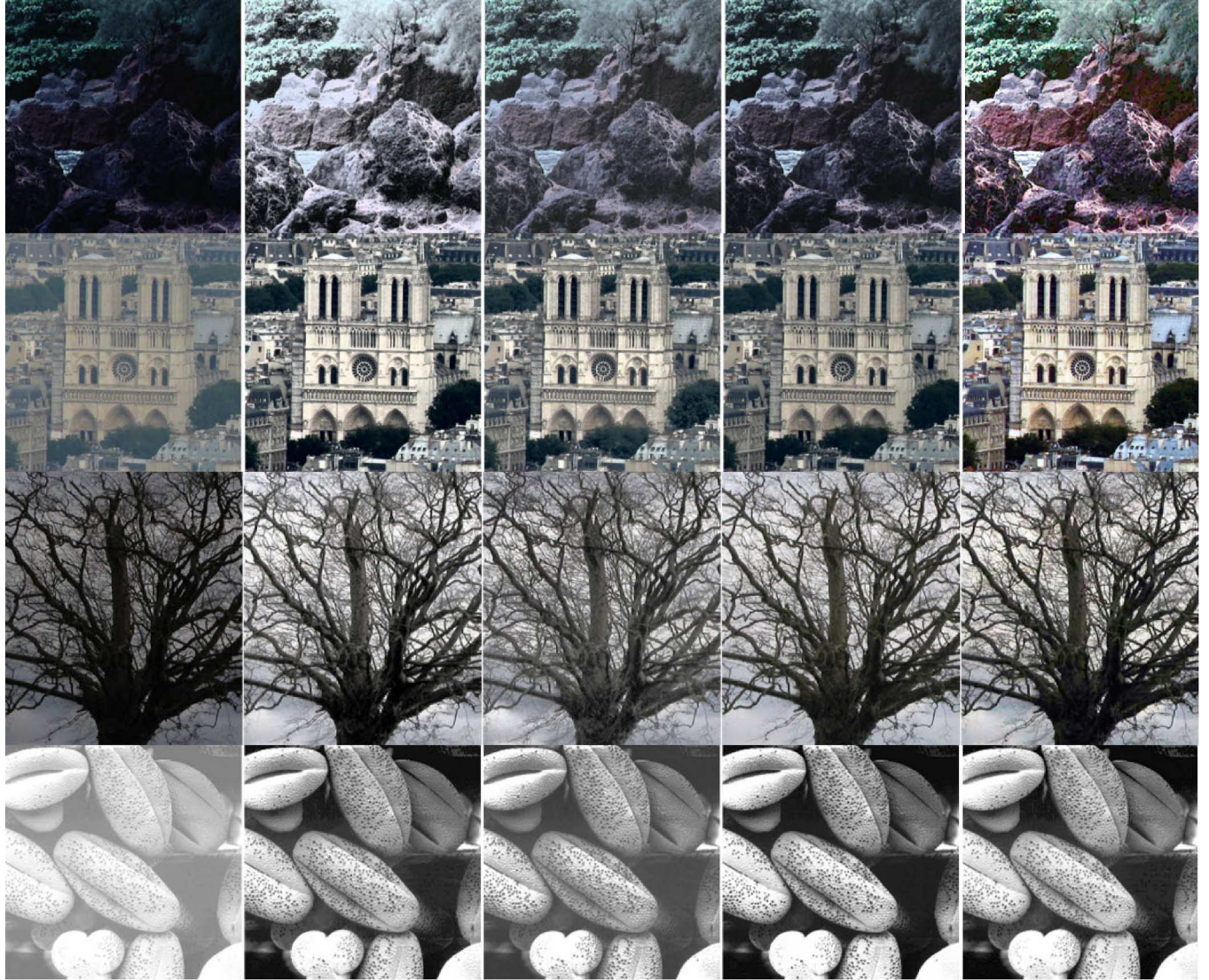


Fig. 8. The columns from left to right are: original images; the histogram equalization results; the enhancement results gotten by CLAHE [9]; the results of OCTM [43]; and the results gotten by the proposed method. Experimental results of other algorithms come from [43] directly.

Theorem 1 tells us that if $\beta = 0$, the effect of (12) will be equal to adjusting s_i to a same length no matter what n is chosen. In such a situation, s_i has nothing to do with p_i .

When $\beta > 0$, the l_n balls become axial symmetric and the optimal points move from the center of the feasible domain to its boundary. In Fig. 2 the optimal solution of $\min -l_1$ is obvious, i.e. as long as $\beta > 0$, the optimal point is $(d, L-d)$. This means that the solution of the l_1 form of (12) is equivalent to that of (7), which is sparse. On the other hand, the optimal solutions in the l_2 and l_∞ cases converge to the boundary of the feasible domain gradually with the increase of β . So, we promote the conclusion to the general situation and then get another theorem.

Theorem 2: Supposing the sparse solution of (12) with $n = 1$ is \mathbf{s}_b . The minima of $\|\mathbf{P}^{-\beta}\mathbf{s}\|_n, n = 2, \infty$, converges to \mathbf{s}_b with the increase of β . The rate of convergence of $n = 2$ is the square of the rate of $n = \infty$.

According to Theorem 2, the convergence point of the solution in the case of $n = 2$ is the same with that of $n = \infty$. The

only difference is the convergence rate. Furthermore, in generalized equalization model, we get

$$\mathbf{G}_1 = \frac{L p_m}{C_{ori}}, \quad \mathbf{G}_2 = \frac{L \|\mathbf{p}^{2\beta+1}\|_1}{C_{ori} \|\mathbf{p}^{2\beta}\|_1}, \quad \mathbf{G}_\infty = \frac{L \|\mathbf{p}^{\beta+1}\|_1}{C_{ori} \|\mathbf{p}^\beta\|_1}, \quad (14)$$

where p_m is the largest element in \mathbf{p} and C_{ori} is the expected contrast of original image.

$$NL_1 \approx \sqrt{2}L,$$

$$NL_2 \approx \frac{L}{\sum_{k=1}^K p_k^{2\beta}} \sqrt{\sum_{j=1}^{K-1} (p_{j+1}^{2\beta} - p_j^{2\beta})^2} = \frac{L \|\nabla \mathbf{p}^{2\beta}\|_2}{\|\mathbf{p}^{2\beta}\|_1},$$

$$NL_\infty \approx \frac{L}{\sum_{k=1}^K p_k^\beta} \sqrt{\sum_{j=1}^{K-1} (p_{j+1}^\beta - p_j^\beta)^2} = \frac{L \|\nabla \mathbf{p}^\beta\|_2}{\|\mathbf{p}^\beta\|_1}.$$



Fig. 9. To each sub-figure, the left one shows original image which has obvious tonal distortion. The right one is the result gotten by the proposed method. The first six test images come from the network resource of Nagasaki University library.



Fig. 10. To each sub-figure, the left one shows original under-exposed images and the right one is the results gotten by the proposed method.

The equations above show that besides the solution of (12), β also controls the contrast gain and the nonlinearity of the proposed model. Similar to the conclusion given in Theorem 2, we can deduce Theorem 3³.

Theorem 3: The contrast G_2 and G_∞ converge to G_1 with the increase of β , and the rate of convergence of G_2 is the square of that of G_∞ . Similarly, the nonlinearity NL_2 and NL_∞ converge to NL_1 with the increase of β , and the rate of convergence of NL_2 is the square of that of NL_∞ .

³The proofs of theorem 3 are similar to those of theorem 2, so we do not repeat it in the Appendix.

Theorem 2 and 3 provide the guidance for the choice of n and β . When $n < 1$, (12) is a non-convex problem, whose solution is sparse and can be achieved by relaxing to $n = 1$. On the other hand, when $n > 1$, the problem is convex, the solution converges to that of $n = 1$, with the increase of β . It means that n must be larger than 1, so that (12) can avoid sparse solution. From this view, we choose $n = 2$ in the proposed model.

Besides n , we also need to choose an optimal value for β so that the enhanced image would have high contrast gain and low nonlinearity of transform. To achieve that goal, we enhance 400 images by generalized equalization model with different

TABLE III
MEDIAN ANGULAR ERROR (DEGREE) ON THREE DATA SETS FOR VARIOUS COLOR CONSTANCY METHODS

Configuration of Proposed Method	Equivalent	Indoor Image Set [3]	Real-World Set [6]	HDR Set [20]
$n = \infty, \alpha = 1, \beta = 0$	Gray-World[4]	7.1	6.2	7.5
$n = \infty, \alpha = \infty, \beta = 0$	Max-RGB[28]	6.5	5.1	3.0
$n = \infty, \alpha = 7, \beta = 0$	Shades of Gray[17]	3.7	4.5	2.9
-	Gray-Edge[40]	3.7	4.6	2.8

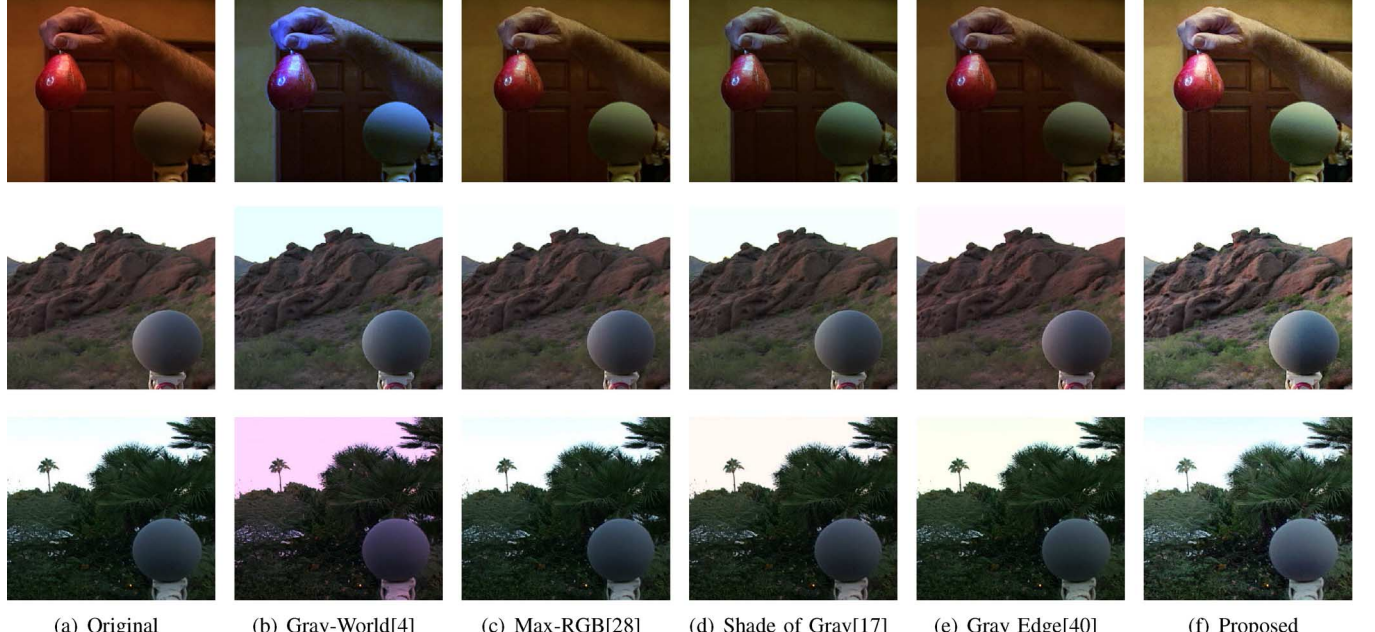


Fig. 11. Comparison of traditional white balancing methods and the proposed method on the real world data set [6]. (a) Original; (b) Gray-World [4]; (c) Max-RGB [28]; (d) Shade of Gray [17]; (e) Gray Edge [40]; (f) Proposed.

β s. Given enhanced images, we plot the average curves of the expected contrast gain, the nonlinearity of transform and the ratio between them respectively, as Fig. 3 shows.

In the Fig. 3, both \mathbf{G}_n and \mathbf{NL}_n increase with β . It means that a large β leads to the strong enhancement of contrast. However, the nonlinearity of transform is serious at the same time, which increases the risk of tone distortion. Fortunately, the ratio of \mathbf{NL}_n to \mathbf{G}_n has an obvious minimum, which means that we can choose β such that the nonlinearity of transform is small enough while the contrast gain is large enough. So the optimal β can be achieved by minimizing following objective.

$$\hat{\beta} = \min_{\beta} \frac{\mathbf{NL}_n}{\mathbf{G}_n}. \quad (15)$$

In Fig. 3(c), the optimal $\hat{\beta}$ is about 0.32 when $n = 2$ and 0.64 when $n = \infty$, which can be used as the default configuration of the proposed model.

Fig. 4 gives different enhancement results and corresponding histograms with different selections of β . In (12), \hat{s} is approximately proportional to \mathbf{p}^{β} . Although the contrast gain increases with β , the visual effect under large β is often not visually pleasant—unreasonable large elements in \hat{s} occupy too large range while small elements causes the fusion of bins in the final histogram. As a result, the image is over-enhanced, which contains obvious artifacts. Recall the finding that when $n = 2$, $\beta =$

0.5, the result is equal to that of histogram equalization. Considering the fact that histogram equalization tends to over-enhance the original image, the optimal value of β in Fig. 3(c) is reasonable.

B. The Choice of α

According to the work in [17], [40], α reflects the hypothesis used for color constancy. In the generalized equalization model the upper bound L_c is chosen by color constancy algorithm. The selection of the optimal α for image enhancement is still based on the minima of $\mathbf{NL}_n/\mathbf{G}_n$. For the convenience of analysis, here we let $n = 2$. In the $\alpha\beta$ -plane, as Fig. 5 shows, we plot the expected contrast gain, the non-linearity of the transform and the ratio of them as the functions of α, β . With the increase of α , 1) both \mathbf{G}_2 and \mathbf{NL}_2 increase; 2) at the same time, the minima of $\mathbf{NL}_2/\mathbf{G}_2$ becomes lower and its location shifts along the reducing direction of β slowly. When $\alpha = \infty$, $\mathbf{NL}_2/\mathbf{G}_2$ achieves the minimum value. It means that the upper bound of intensity of each channel in (12) is estimated by max-RGB. In fact, the efficiency of max-RGB method to color constancy problem is proven in [19], [20], which provides us with a strong support to our choice.

C. Summary of The Model

The generalized equalization model achieves the desired purposes as mentioned in the beginning of this section. 1) Both



Fig. 12. From left to right: Figure (a) includes the original image, the result gotten by the proposed method, the result in [21], and the results gotten by Gray-world, max-RGB, Shade of Gray and Edge-Gray. Figure (b) includes the original images, the results gotten by the proposed method, the results in [41], and the results gotten by Gray-world, max-RGB, Shade of Gray and Edge-Gray. Figure (c) includes the raw camera images, the proposed method's results, the correction results based on measured illuminant, and the results gotten by Gray-world, max-RGB, Shade of Gray and Edge-Gray. The experimental results of other algorithms come from [15], [21], [41] directly.

white balancing and contrast enhancement problems can be described as transforms of the image histogram. If the transform tends to be linear, the result is closer to the white balancing. Meanwhile, if the transform tends to be nonlinear, the result is closer to contrast enhancement. The generalized equalization model, with suitable parameters, keeps a balance between contrast enhancement (measured by contrast gain) and tonal distortion (measured by nonlinearity of transform). Moreover, it gives a unified framework accommodating many histogram-based image processing algorithms. Under different configurations of parameters, the solution of generalized equalization

model is equivalent to many existing algorithms. Table II⁴ gives a list of the equivalent algorithms corresponding to different configurations of the model parameters.

2) Another advantage of the generalized equalization model is its high efficiency. Eq. (12) is a convex optimization problem that can be solved with mature optimization algorithms and packages. In the case of $n = 2$, the computational complexity of the proposed method is $O(N^2)$. Here N is the number of bins in

⁴When $n = 1$, $\beta = 1$, in order to get the results of OCTM [43], another two constraints of tone should be added. The symbol “-” represents that α can be arbitrary positive real number.

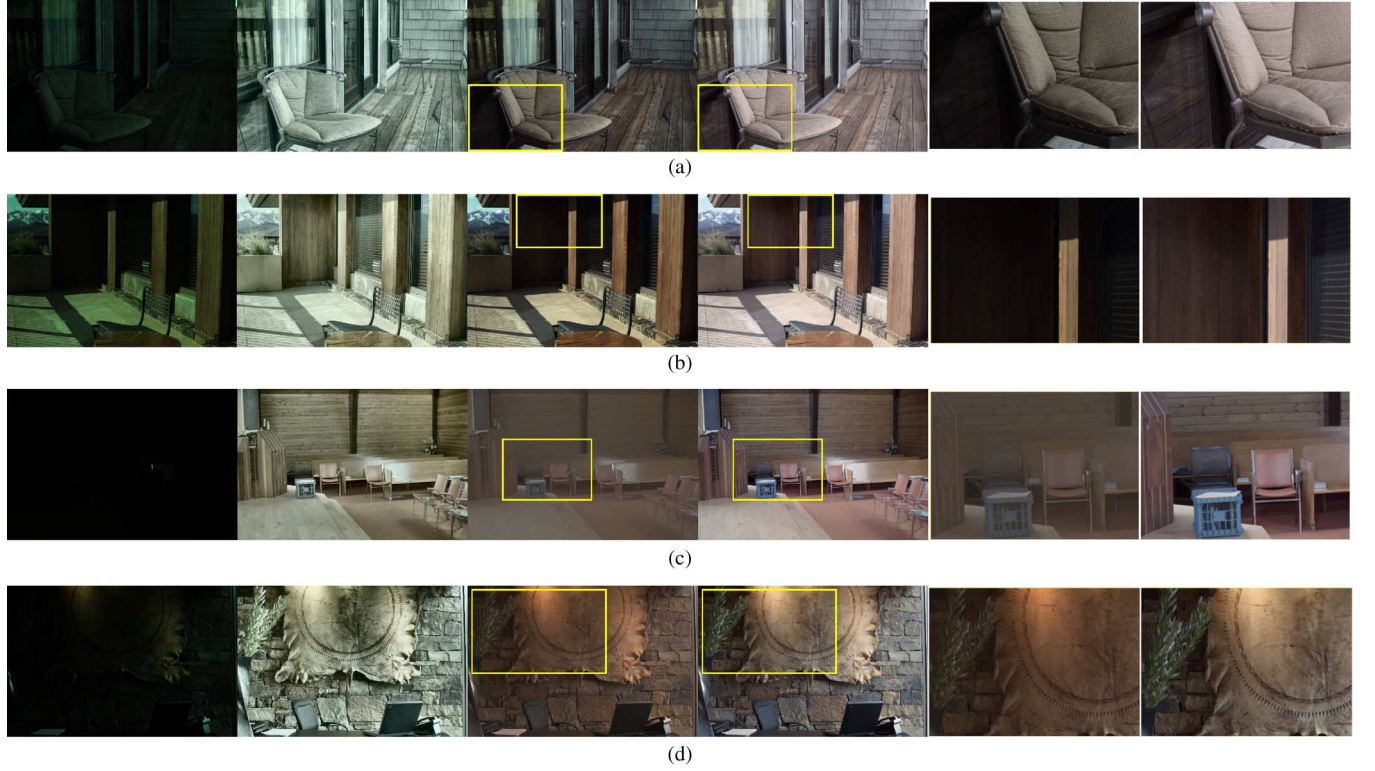


Fig. 13. In sub-figure (a,b), the image from left to right are original image, the default tone mapping result, the result of gamma correction with $\gamma = 0.8$, the result of proposed method and enlarged comparison results. In sub-figure (c,d), the image from left to right are original image, the default tone mapping result, the result of gamma correction with $\gamma = 0.4$, the result of proposed method and enlarged comparison results.

the histogram. On the other hand, because OCTM is based on linear programming, its computational complexity is $O(N^3)$. To further illustrate the efficiency of the proposed method, we calculate the processing time of image with different bit lengths (from 8-bit image to 16-bit image) with the help of CVX toolbox [23] and plot the results in Fig. 6. We can find that with the increase of bit length, OCTM consumes much more time than the proposed method.

Additionally, we can accelerate the proposed algorithm further by setting the minimal distance d between adjacent intensity level to 0. In this case, the solution of (12) has an analytic form, which is beneficial for practical applications.

$$h_{ci} = \begin{cases} \frac{L_c \sum_{j=1}^i p_{cj}^{2\beta}}{\sum_{k=1}^K p_{ck}^{2\beta}}, & n = 2 \\ \frac{L_c \sum_{j=1}^i p_{cj}^\beta}{\sum_{k=1}^K p_{ck}^\beta}, & n = \infty, \end{cases} \quad (16)$$

$$L_c = \frac{\sqrt{\sum_{c=r,g,b} \left(\mathbf{p}_c^T \tilde{\mathbf{h}}_c^\alpha \right)^{\frac{2}{\alpha}}}}{\left(\mathbf{p}_c^T \tilde{\mathbf{h}}_c^\alpha \right)^{\frac{1}{\alpha}}} \max(\tilde{\mathbf{h}}_c), \quad (17)$$

$$c = r, g, b.$$

However, it should be mentioned that although setting $d = 0$ can achieve acceleration of algorithm, it brings a risk of merging bins of histogram, which may cause obvious artifacts in some cases.

The parameter β is critical to the proposed model. Instead of solving (15) directly, which is a complicated problem, we proposed a simple strategy to optimize β . In our experiment, the default value $\beta = 0.32$ ($n = 2$) is suitable to most test images. So, we set $\beta = 0.32$ as the initial value and search the optimized value $\hat{\beta}$ by the following steps. Eq. (16) is convenient to compute, even with the iteration scheme above, the processing time is merely 2–3 seconds per image for images of size 512×512 and 8 bit length. The computation is conducted on platform of MATLAB and Intel Core2 CPU. After getting $\hat{\beta}$, we have the corresponding optimally enhance output image.

Optimal Image Enhancement Algorithm

Process:

0. Regard $\mathbf{NL}_2/\mathbf{G}_2$ as a function of β , $F(\beta)$.
1. For $j = 0 : 64$, calculate $F(\beta_j)$, $\beta_j = 0.01j$.
2. Choose $\hat{\beta}$ as the β_j minimizes F .
3. Get the output image corresponding to $\hat{\beta}$.

3) The degree of the freedom of the algorithm is very low. Only 3 parameters are used to control the behavior and performance of the model. This property of low free parameters is highly desirable for interactive semi-automatic image enhancement applications.

TABLE IV
THE \bar{V} OF THE RESULTS IN [10], [13], [26], [37], [38] AND THE \bar{V} OF THE RESULTS IMPROVED BY PROPOSED METHOD

ImageName	Fattal'08[13]		He'09[26]		Kopf'08[10]		Tan'08[37]		Tarel'09[38]	
	Ori	Postprocess	Ori	Postprocess	Ori	Postprocess	Ori	Postprocess	Ori	Postprocess
ny12	1.28	1.51	1.39	1.78	1.40	1.64	2.18	2.65	1.76	2.04
ny17	1.53	1.55	1.62	1.73	1.61	1.65	2.18	2.72	1.70	2.11
y01	1.21	1.44	1.31	1.74	1.63	1.89	2.22	2.85	1.99	2.41
y16	1.20	1.32	1.36	1.67	1.34	1.48	2.06	2.63	1.96	2.33

TABLE V
THE E OF THE RESULTS IN [10], [13], [26], [37], [38] AND THE E OF THE RESULTS IMPROVED BY PROPOSED METHOD

ImageName	Fattal'08[13]		He'09[26]		Kopf'08[10]		Tan'08[37]		Tarel'09[38]	
	Ori	Postprocess	Ori	Postprocess	Ori	Postprocess	Ori	Postprocess	Ori	Postprocess
ny12	-0.054	-0.028	0.048	0.030	0.036	0.054	-0.083	-0.032	0.145	0.130
ny17	-0.106	-0.074	0.023	0.020	0.016	0.026	-0.041	0.109	0.110	0.155
y01	0.086	0.091	0.142	0.143	0.094	0.095	0.122	0.222	0.209	0.191
y16	0.058	0.121	0.131	0.142	0.001	0.044	-0.016	0.039	0.241	0.247

IV. EXPERIMENTAL RESULTS

A. Optimal Contrast Enhancement

A basic application of the proposed algorithm is image contrast enhancement. In the experiments, the configuration of parameters is: $d = 0$, $\alpha = \infty$, $n = 2$. β is chosen according to the optimal image enhancement algorithm introduced in the former section. To demonstrate the validity of the proposed algorithm, we design a subjective experiment. In the experiment, 6 images are given simultaneously in a screen, including the original image from Berkeley Segmentation Dataset (BSDS300), the result corresponding to $\hat{\beta}$ and 4 results with random selected $\beta \in [0, 0.64]$. The 6 images are presented randomly. Each viewer selects the image that he or she thinks has the best visual effect. The experiment is stopped when the viewer does not want to continue. 50 volunteers joined in our subjective viewing experiment. The average number of image tested by each volunteer is 31.3. In our experiment, the probability that a volunteer selects the image corresponding to the optimal β is 65.8%. The average error between $\hat{\beta}$ and β selected subjectively ($\sqrt{(1/N) \sum_{i=1}^N (\hat{\beta}_i - \beta_i)^2}$) is 0.0621. The experimental results show that in most situations, the enhancement results of the proposed method match well with our subjective preference. Fig. 7 shows the errors between subjective β s and the $\hat{\beta}$ s from the proposed algorithm for 300 images in the data set. Compared with $\hat{\beta}$, the error is small in most cases.

Fig. 8 gives the comparison results of the proposed algorithm and some existing methods. We can find that the proposed method achieves the best overall visual effect: it not only enhances the contrast, but also prevents serious nonlinear tonal distortion.

Another database we use is the old pictures in the network resource of Nagasaki University library. We also randomly choose some other images from the Internet. These pictures

suffer not only low contrast but also serious tonal distortion. Using the algorithm based on generalized equalization model, we can achieve contrast enhancement and white balancing jointly, as illustrated in Fig. 9. We also test the proposed method on under-exposed images, as shown in Fig. 10. With the help of the proposed method, the details in the dark region become clearer.

B. Joint White Balancing and Enhancement

According to Table II, when β is close to 0, the behavior of the proposed method is close to white balancing. To demonstrate performance of the proposed method in white balancing, we test the proposed method on three color constancy data sets. The angular error between the estimated light source $\hat{\mathbf{e}}$ and the ground truth \mathbf{e}_l is calculated as $\arccos(\hat{\mathbf{e}} \cdot \mathbf{e}_l)$. Table III gives the median angular error on three data sets [3], [6], [20] for various color constancy methods. Compared with gray-edge method, under suitable configuration, our method provides comparable color constancy results.

As a major contribution, the generalized equalization model provides a joint strategy for image enhancement. If we relax β to a small positive number, we can combine white balancing and enhancement into an integrated algorithm. In Fig. 11 and 12, we compare the proposed method with some existing white balancing algorithms, where we can see that the proposed method not only corrects the tone bias in original images but also enhances the contrast.

C. Global Tone Mapping for HDR Image

Tone mapping for HDR Image is another natural application for the proposed model. Many tone mapping algorithms have been proposed through the years, e.g. those in [1], [5], [7], [11], [14], [24], [27], [36], [39]. Although the methods [11], [14], [27], [39] based on local adaptive filtering achieve encouraging



Fig. 14. Figure (a) gives comparison between de-hazing result of [26] and the result after adding post-processing. Figure (b) gives comparison between de-hazing result of [38] and the result after adding post-processing. Figure (c) gives comparison between de-hazing result of [10] and the result after adding post-processing.

results, the global method, such as gamma correction, is still the most popular choice because of its robustness and lower complexity. We test our method on the HDR images captured by Nikon D700⁵ and map them into 8-bit and compare the results with those from the default tone mapping process in MATLAB and gamma correction.

Although the default tone mapping in MATLAB can reveal some image details, it cannot recover the color of image correctly. In other words, the contrast is enhanced but the tone bias is raised. On the other hand, gamma correction avoids obvious tone bias and protects the color of image but suffers from inap-

propriate choice of γ : if γ is close to 1, the details in the dark region of image will not be visible, as Fig. 13(a), (b) shows; if γ is close to 0, the contrast of image will be reduced, as Fig. 13(c), (d) shows. Compared with the MATLAB tone mapping and gamma correction, the proposed model clearly gives more visually pleasant results, as shown in Fig. 13.

D. Post-Processing for De-hazing Algorithm

The proposed method is also suitable for post-processing of many existing enhancement algorithms. For example, although the existing de-hazing algorithms can remove the needless white-light components in the background of the images, they

⁵The data set is taken from http://www.cs.sfu.ca/~colour/data/funt_hdr/.

may lead to tonal distortion in the foreground. So, we can apply the proposed method as a post-processing step of the de-hazing algorithms to rectify the tonal distortion.

To evaluate the performance of our method, we apply the two blind contrast restoration assessment methods described in [25], namely the increase of the number of visible edge, E , and the mean of the visibility level, \bar{V} . We denote the number of visible edge in original image and that in processing result as N_o and N_r respectively. The increase of visible edge is denoted as $E = N_r - N_o/N_o$. The larger E we get, the better the performance of contrast enhancement. Similarly, the increase of the value of \bar{V} also indicates the enhancement of visibility of an image. Because the definition of \bar{V} is out of the range of this paper, we refer the reader to [25] and the code on the website <http://perso.lcpc.fr/tarel.jean-philippe/visibility/> for the details of this descriptor.

Using test images from: <http://perso.lcpc.fr/tarel.jean-philippe/visibility/>, we first calculate the values of E and \bar{V} for the de-hazing methods [10], [13], [26], [37], [38]. Then, we use the proposed method as a post-processing step and calculate E and \bar{V} again. Table IV and V give the results of \bar{V} and E respectively.

After incorporating the proposed method as post-processing step, most E and all the \bar{V} of de-hazing results are improved. This experimental result indicates that the proposed method can further improve the visual results of those de-hazing algorithms.

Besides the objective experiment given above, we also design a subjective view test to verify the human-centered performance of our proposed model. In the experiment, a hazed image is processed respectively by two methods—a method selected from [13], [26], [37], [38] and the selected method combined with post-processing using our proposed model. Then those three images are sorted randomly and displayed simultaneously in a screen. Each viewer selects the image that he/she thinks having the best visual effect. The experiment is stopped whenever the viewer does not want to continue. The selection of de-hazing algorithm is random and unknown for each participant.

30 viewers are involved in our experiment. The average number of image tested by each volunteer is 7.8. In our experiment, the probability that volunteers select the image corresponding to the method combined with our post-processing step is 95.8%. This result shows that in most situations, the enhancement results of the proposed method cater our subjective feelings better. Fig. 14 gives more examples of the processing results for the readers' evaluation.

V. CONCLUSION

In this paper, we analyzed the relationships between image histogram and contrast/tone. We established a generalized equalization model for global image tone mapping. Extensive experimental results suggest that the proposed method has good performances in many typical applications including image contrast enhancement, tone correction, white balancing and post-processing of de-hazed images. In the future, besides global image enhancement, we expect to unify more local image enhancement methods into the model through local image feature analysis.

APPENDIX

The Proof of Theorem 1:

Proof: When $\beta = 0$, $\|\mathbf{P}^{-\beta}\mathbf{s}\|_n = \|\mathbf{s}\|_n$. Define $\mathbf{s}_o = [L/K, \dots, L/K]$ as a K dimensional vector, which is the optimal solution of (12). Assume that there exists another vector $\mathbf{s}' \neq \mathbf{s}_o$ satisfying $\|\mathbf{s}'\|_n < \|\mathbf{s}_o\|_n$. According to the constraint that $\sum_{i=1}^K s_i = L$, at least one of the element of \mathbf{s}' is larger than L/K , which can be labeled as s'_l . Then we have

$$\|\mathbf{s}'\|_1 = L = \|\mathbf{s}_o\|_1, \quad \|\mathbf{s}'\|_\infty = s'_l > \frac{L}{K} = \|\mathbf{s}_o\|_\infty.$$

Because $\|\mathbf{s}\|_2$ is convex, we have

$$\|\mathbf{s}'\|_2 > \sqrt{K(\bar{\mathbf{s}}')^2} = \frac{L}{\sqrt{K}} = \|\mathbf{s}_o\|_2.$$

Here $\bar{\mathbf{s}}'$ is the mean of \mathbf{s}' . As a result, the assumption is false and therefore this theorem is proven. \square

The Proof of Theorem 2: The rate of convergence of function f , whose limit is \hat{f} is defined as

$$Q = \lim_{t \rightarrow \infty} \frac{\|f_{t+1} - \hat{f}\|_2}{\|f_t - \hat{f}\|_2}.$$

When $0 < Q < 1$, f is linear convergent to its limit.

Proof: We can assume that $p_i \leq p_{i+1}$, $i = 1, \dots, K$, without loss of generality. Define the optimal solutions of the l_2 and l_∞ forms of (12) as \mathbf{s}_2 and \mathbf{s}_∞ . Then we have

$$\mathbf{s}_2 = \frac{L}{\sum_{i=1}^K p_i^{2\beta}} [p_1^{2\beta}, \dots, p_K^{2\beta}], \quad \mathbf{s}_\infty = \frac{L}{\sum_{i=1}^K p_i^\beta} [p_1^\beta, \dots, p_K^\beta].$$

Both of them are functions of β , whose limits are $\mathbf{L} = [L, 0, \dots, 0]$.

The rates of convergence corresponding to \mathbf{s}_2 and \mathbf{s}_∞ are denoted as Q_2 and Q_∞ respectively. According to the definition of Q , we have

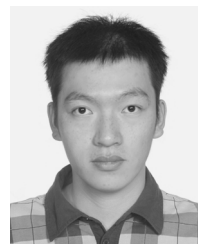
$$\begin{aligned} Q_2 &= \lim_{\beta \rightarrow \infty} \frac{\|\mathbf{s}_{2(\beta+1)} - \mathbf{L}\|_2}{\|\mathbf{s}_{2(\beta)} - \mathbf{L}\|_2} \\ &= \lim_{\beta \rightarrow \infty} \frac{\sum_{i=1}^K p_i^{2\beta}}{\sum_{i=1}^K p_i^{2\beta+2}} \cdot \sqrt{\frac{\|\mathbf{p}^{2\beta+2}\|_1^2 + \|\mathbf{p}^{4\beta+4}\|_1}{\|\mathbf{p}^{2\beta}\|_1^2 + \|\mathbf{p}^{4\beta}\|_1}} \\ &= \frac{1}{p_1^2} \sqrt{\frac{K(K-1)p_2^{4\beta+4}}{K(K-1)p_2^{4\beta}}} = \frac{p_2^2}{p_1^2}. \end{aligned}$$

Similarly, we can get $Q_\infty = p_2/p_1$. Because $0 < Q_2 = Q_\infty^2 < 1$, both of the solutions converge to \mathbf{L} linearly, and the rate of convergence of $n = 2$ is the square of the rate of $n = \infty$. \square

REFERENCES

- [1] T. Arici, S. Dikbas, and Y. Altunbasak, "A histogram modification framework and its application for image contrast enhancement," *IEEE Trans. Image Process.*, vol. 18, no. 9, pp. 1921–1935, 2009.
- [2] M. Ashikhmin, "A tone mapping algorithm for high contrast images," in *Proc. 13th Eurographics Workshop Rendering*, 2002.
- [3] K. Barnard, L. Martin, B. Funt, and A. Coath, "A data set for colour research," *Color Res. Applicat.*, vol. 27, no. 3, pp. 147–151, 2002.

- [4] G. Buchsbaum, "A spatial processor model for object colour perception," *J. Frank. Inst.*, vol. 310, 1980.
- [5] Z. Chen, B. Abidi, D. Page, and M. Abidi, "Gray-level grouping (glg): An automatic method for optimized image contrast enhancement—Part i: The basic method," *IEEE Trans. Image Process.*, vol. 15, no. 8, pp. 2303–2314, 2006.
- [6] F. Ciurea and B. Funt, The SunBurst Resort, Scottsdale, AZ, USA, "A large image database for color constancy research," in *Proc. IS&T/SID's Color Imaging Conf.*, 2004, pp. 160–164.
- [7] D. Coltuc, P. Bolon, and J.-M. Chassery, "Exact histogram specification," *IEEE Trans. Image Process.*, vol. 15, no. 5, pp. 1143–1152, 2006.
- [8] F. Drago, K. Myszkowski, T. Annen, and N. Chiba, "Adaptive logarithmic mapping for displaying high contrast scenes," in *Proc. Computer Graphics Forum*, 2003, vol. 22, no. 3.
- [9] E. D. P. et al., "Contrast limited adaptive histogram image processing to improve the detection of simulated speculations in dense mammograms," *J. Digital Imag.*, vol. 11, no. 4, pp. 193–200, 1998.
- [10] J. K. et al., "Deep photo: Model-based photograph enhancement and viewing," *ACM Trans. Graph.—Proc. ACM SIGGRAPH*, vol. 27, no. 5, 2008.
- [11] Z. Farbman, R. Fattal, D. Lischinski, and R. Szeliski, "Edge-preserving decompositions for multi-scale tone and detail manipulation," *ACM Trans. Graph.*, vol. 27, no. 3, 2008.
- [12] H. Farid, "Blind inverse gamma correction," *IEEE Trans. Image Process.*, vol. 10, no. 10, pp. 1428–1433, 2001.
- [13] R. Fattal, "Single image dehazing," *ACM Trans. Graph.—Proc. ACM SIGGRAPH*, vol. 27, no. 3, 2008.
- [14] R. Fattal, M. Agrawala, and S. Rusinkiewicz, "Multiscale shape and detail enhancement from multi-light image collections," *ACM Trans. Graph.*, vol. 26, no. 3, pp. 51–59, 2007.
- [15] G. Finlayson and S. Hordley, "A theory of selection for gamut mapping colour constancy," in *Proc. IEEE Int. Conf. Computer Vision and Pattern Recognition*, 1998, pp. 60–65.
- [16] G. Finlayson, S. Hordley, and P. Hubel, "Colour by correlation: A simple, unifying approach to colour constancy," in *Proc. IEEE Int. Conf. Computer Vision*, 1999, vol. 2, pp. 835–842.
- [17] G. Finlayson and E. Trezzi, "Shades of gray and colour constancy," in *Proc. IS&T/SID 12th Color Imaging Conf.*, 2004, pp. 37–41.
- [18] D. Forsyth, "A novel algorithm for color constancy," *Int. J. Comput. Vision*, vol. 5, no. 1, pp. 5–36, 1990.
- [19] B. Funt and L. Shi, "The effect of exposure on maxrgb color constancy," in *Proc. SPIE Volume 7527, Human Vision and Electronic Imaging*.
- [20] B. Funt and L. Shi, "The rehabilitation of maxrgb," in *Proc. IS&T 18th Color Imaging Conf.*
- [21] P. Gehler, C. Rother, A. Blake, T. Minka, and T. Sharp, "Bayesian color constancy revisited," in *Proc. IEEE Int. Conf. Computer Vision and Pattern Recognition*, 2008, pp. 1–8.
- [22] R. C. Gonzalez and R. E. Woods, *Digital Image Processing*. Beijing, China: Publishing House of Electronics Industry, 2002.
- [23] M. Grant and S. Boyd, CVX users guide, Technical report, Information Systems Laboratory, Department of Electrical Engineering, Stanford University, 2009.
- [24] J.-H. Han, S. Yang, and B.-U. Lee, "A novel 3-d color histogram equalization method with uniform 1-d gray scale histogram," *IEEE Trans. Image Process.*, vol. 20, no. 2, pp. 506–512, 2011.
- [25] N. Hautière, J.-P. Tarel, D. Aubert, and E. Dumont, "Blind contrast restoration assessment by gradient rationing at visible edges," in *Proc. Int. Congr. Stereology (ICS'07)*, Saint Etienne, France, 2007 [Online]. Available: <http://perso.lcpc.fr/tarel.jean-philippe/publis/ics07.html>
- [26] K. He, J. Sun, and X. Tang, "Single image haze removal using dark channel prior," in *Proc. IEEE Int. Conf. Computer Vision and Pattern Recognition*, 2009, pp. 1956–1963.
- [27] K. He, J. Sun, and X. Tang, "Guided image filtering," in *Proc. ECCV*, 2010.
- [28] E. Land and J. McCann, "Lightness and retinex theory," *J. Opt. Soc. Amer. A*, vol. 61, no. 1, pp. 1–11, 1971.
- [29] P. Ledda, A. Chalmers, T. Troscianko, and H. Seetzen, "Evaluation of tone mapping operators using a high dynamic range display," *ACM Trans. Graph.—Proc. ACM SIGGRAPH*, vol. 24, no. 3, 2005.
- [30] P. Milanfar, "A tour of modern image filtering: New insights and methods, both practical and theoretical," *IEEE Signal Process. Mag.*, vol. 30, no. 1, pp. 106–128, 2013.
- [31] S.-C. Pei, Y.-C. Zeng, and C.-H. Chang, "Virtual restoration of ancient Chinese paintings using color contrast enhancement and lacuna texture synthesis," *IEEE Trans. Image Process.*, vol. 13, no. 3, pp. 416–429, 2004.
- [32] Y.-F. Pu, J.-L. Zhou, and X. Yuan, "Fractional differential mask: A fractional differential-based approach for multiscale texture enhancement," *IEEE Trans. Image Process.*, vol. 19, no. 2, pp. 491–511, 2010.
- [33] E. Reinhard, M. Stark, P. Shirley, and J. Ferwerda, "Photographic tone reproduction for digital images," *ACM Trans. Graph.—Proc. ACM SIGGRAPH*, vol. 21, no. 3, 2002.
- [34] Y. Shi, J. Yang, and R. Wu, "Reducing illumination based on nonlinear gamma correction," in *Proc. IEEE Int. Conf. Image Processing*, 2007, vol. 1, pp. 529–532.
- [35] J.-L. Starck, F. Murtagh, E. Candès, and D. Donoho, "Gray and color image contrast enhancement by the curvelet transform," *IEEE Trans. Image Process.*, vol. 12, no. 6, pp. 706–717, 2003.
- [36] J. A. Stark, "Adaptive image contrast enhancement using generalizations of histogram equalization," *IEEE Trans. Image Process.*, vol. 9, no. 5, pp. 889–896, 2000.
- [37] R. Tan, "Visibility in bad weather from a single image," in *Proc. IEEE Int. Conf. Computer Vision and Pattern Recognition*, 2008, pp. 1–8.
- [38] J.-P. Tarel and N. Hautiere, "Fast visibility restoration from a single color or gray level image," in *Proc. IEEE Int. Conf. Computer Vision*, 2009, pp. 2201–2208.
- [39] C. Tomasi and R. Manduchi, "Bilateral filtering for gray and color images," in *Proc. ICCV*, 1998.
- [40] J. van de Weijer, T. Gevers, and A. Gijsenij, "Edge-based color constancy," *IEEE Trans. Image Process.*, vol. 16, no. 9, pp. 2207–2214, 2007.
- [41] J. van de Weijer, C. Schmid, and J. Verbeek, "Using high-level visual information for color constancy," in *Proc. IEEE Int. Conf. Computer Vision*, 2007, pp. 1–8.
- [42] Y. Wang, Q. Chen, and B. Zhang, "Image enhancement based on equal area dualistic sub-image histogram equalization method," *IEEE Trans. Consum. Electron.*, vol. 45, no. 1, pp. 68–75, 1999.
- [43] X. Wu, "A linear programming approach for optimal contrast-tone mapping," *IEEE Trans. Image Process.*, vol. 20, no. 5, pp. 1262–1272, 2010.
- [44] X. Zhu and P. Milanfar, "Restoration for weakly blurred and strongly noisy images," in *Proc. 2011 IEEE Workshop Applications of Computer Vision (WACV)*, 2011, pp. 103–109.



Hongteng Xu received the B.S. degree from Tianjin University, Tianjin, China, in 2010. In fall 2010, he joined in the dual-master program of Georgia Institute of Technology and Shanghai Jiao Tong University, and graduated in Spring 2013.

Currently, he is a Ph.D. student, School of Electrical and Computer Engineering, Georgia Tech. His research interests include image processing, computer vision, data mining and machine learning.



Guangtao Zhai (M'10) received the B.E. and M.E. degrees from Shandong University, Shandong, China, in 2001 and 2004 and the Ph.D. degree from Shanghai Jiao Tong University, Shanghai, China, in 2009.

He is currently a research professor at the Institute of Image Communication and Information Processing, Shanghai Jiao Tong University, Shanghai, China. From August 2006 to February 2007, he was a Student Intern with the Institute for Infocomm Research, Singapore. From March 2007 to January 2008, he was a Visiting Student with the School of Computer Engineering, Nanyang Technological University, Singapore. From October 2008 to April 2009, he was a Visiting Student with the Department of Electrical and Computer Engineering, McMaster University, Hamilton, ON, Canada, where from January 2010 to March 2012 he was a Postdoctoral Fellow. His research interests include multimedia signal processing and perceptual signal processing.



Xiaolin Wu (M'88–SM'96–F'11) received the B.Sc. degree in computer science from Wuhan University, Wuhan, China, in 1982, and the Ph.D. degree in computer science from the University of Calgary, Calgary, AB, Canada, in 1988. He started his academic career in 1988 and has since been on the faculty of the University of Western Ontario, New York Polytechnic University, and McMaster University, Hamilton, ON, Canada, where he is a Professor in the Department of Electrical and Computer Engineering and holds the NSERC-DALSA

Industrial Research Chair in Digital Cinema. Currently, he is also with the institute of image communication and information processing, Shanghai Jiao Tong University, Shanghai, China. His research interests include image processing, multimedia compression, joint source-channel coding, multiple description coding, and network-aware visual communication. He has published over 180 research papers and holds two patents in these fields.

Dr. Wu was an Associate Editor of the IEEE TRANSACTIONS ON MULTIMEDIA. He is an Associate Editor of the IEEE TRANSACTIONS ON IMAGE PROCESSING.



Xiaokang Yang (M'00–SM'04) received the B. S. degree from Xiamen University, Xiamen, China, in 1994, the M. S. degree from Chinese Academy of Sciences, Shanghai, China, in 1997, and the Ph.D. degree from Shanghai Jiao Tong University, Shanghai, China, in 2000.

He is currently a professor and Vice Dean, School of Electronic Information and Electrical Engineering, and the deputy director of the Institute of Image Communication and Information Processing, Shanghai Jiao Tong University, Shanghai, China.

From August 2007 to July 2008, he visited the Institute for Computer Science, University of Freiburg, Germany, as an Alexander von Humboldt Research Fellow. From September 2000 to March 2002, he worked as a Research Fellow in Centre for Signal Processing, Nanyang Technological University, Singapore. From April 2002 to October 2004, he was a Research Scientist in the Institute for Infocomm Research, Singapore. He has published over 150 refereed papers, and has filed 30 patents. His current research interests include visual signal processing and communication, media analysis and retrieval, and pattern recognition.

He received National Science Fund for Distinguished Young Scholars in 2010, Professorship Award of Shanghai Special Appointment (Eastern Scholar) in 2008, the Microsoft Young Professorship Award in 2006, the Best Young Investigator Paper Award at IS&T/SPIE International Conference on Video Communication and Image Processing (VCIP2003) and awards from A-STAR and Tan Kah Kee foundations. He is currently a member of Editorial Board of IEEE Signal Processing Letters, Series Editor of Springer CCIS, a member of APSIPA, a senior member of IEEE, a member of Visual Signal Processing and Communications (VSPC) Technical Committee of the IEEE Circuits and Systems Society. He was the special session chair of Perceptual Visual Processing of IEEE ICME2006. He was the technical program co-chair of IEEE SiPS2007 and the technical program co-chair of 3DTV workshop in junction with 2010 IEEE International Symposium on Broadband Multimedia Systems and Broadcasting.